REPORTS

SOLID-STATE PHYSICS

Scalable T^2 resistivity in a small single-component Fermi surface

Xiao Lin, Benoît Fauqué, Kamran Behnia*

Scattering among electrons generates a distinct contribution to electrical resistivity that follows a quadratic temperature (T) dependence. In strongly correlated electron systems, the prefactor A of this T^2 resistivity scales with the magnitude of the electronic specific heat, γ. Here we show that one can change the magnitude of A by four orders of magnitude in metallic strontium titanate ($SrTiO_3$) by tuning the concentration of the carriers and, consequently, the Fermi energy. The T^2 behavior persists in the single-band dilute limit despite the absence of two known mechanisms for T^2 behavior: distinct electron reservoirs and Umklapp processes. The results highlight the absence of a microscopic theory for momentum decay through electron-electron scattering in various Fermi liquids.

Warming a metal enhances its resistivity because scattering events along the trajectory of a charge-carrying electron become more frequent with increasing temperature (T). In most simple metals, the dominant mechanism is scattering by phonons, leading to a T^5 dependence of resistivity. In 1937, Baber identified electron-electron scattering as the origin of T^2 resistivity observed in many transition metals (*1*). During the past few decades, it has been firmly established that, at low temperatures, resistivity (ρ) in a Fermi liquid follows a quadratic temperature dependence expressed as $\rho = \rho_0 + AT^2$ (where A is the prefactor of the T^2 resistivity) and that correlations among electrons enhance both A and the electronic specific heat, γ. This is often expressed through the Kadowaki-Woods ratio ($R_{KW} = A/\gamma^2$) (*2*–*6*), which links two distinct properties of a Fermi liquid, each set by the same material-dependent Fermi energy, E_F.

The Pauli exclusion principle is the ultimate reason behind both the T-linear specific heat and T-square resistivity in Fermi liquids. Electrons that give rise to both properties are those confined to a width of k_BT/E_F, where k_B is the Boltzmann constant. In the case of resistivity, this is true of both electrons participating in the scattering event, hence the exponent of two. However, electron-electron scattering alone does not generate a finite contribution to resistivity, because such a scattering event would conserve momentum with no decay in the charge current. The presence of an underlying lattice is required in any scenario for generating T^2 resistivity from electron-electron scattering. Dimensional considerations imply

$$A = \frac{\hbar}{e^2}\left(\frac{k_B}{E_F}\right)^2 \ell_{quad} \quad (1)$$

Laboratoire de Physique et Etude des Matériaux (CNRS/UPMC), Ecole Supérieure de Physique et de Chimie Industrielles, 10 Rue Vauquelin, F-75005 Paris, France.
*Corresponding author. E-mail: kamran.behnia@espci.fr

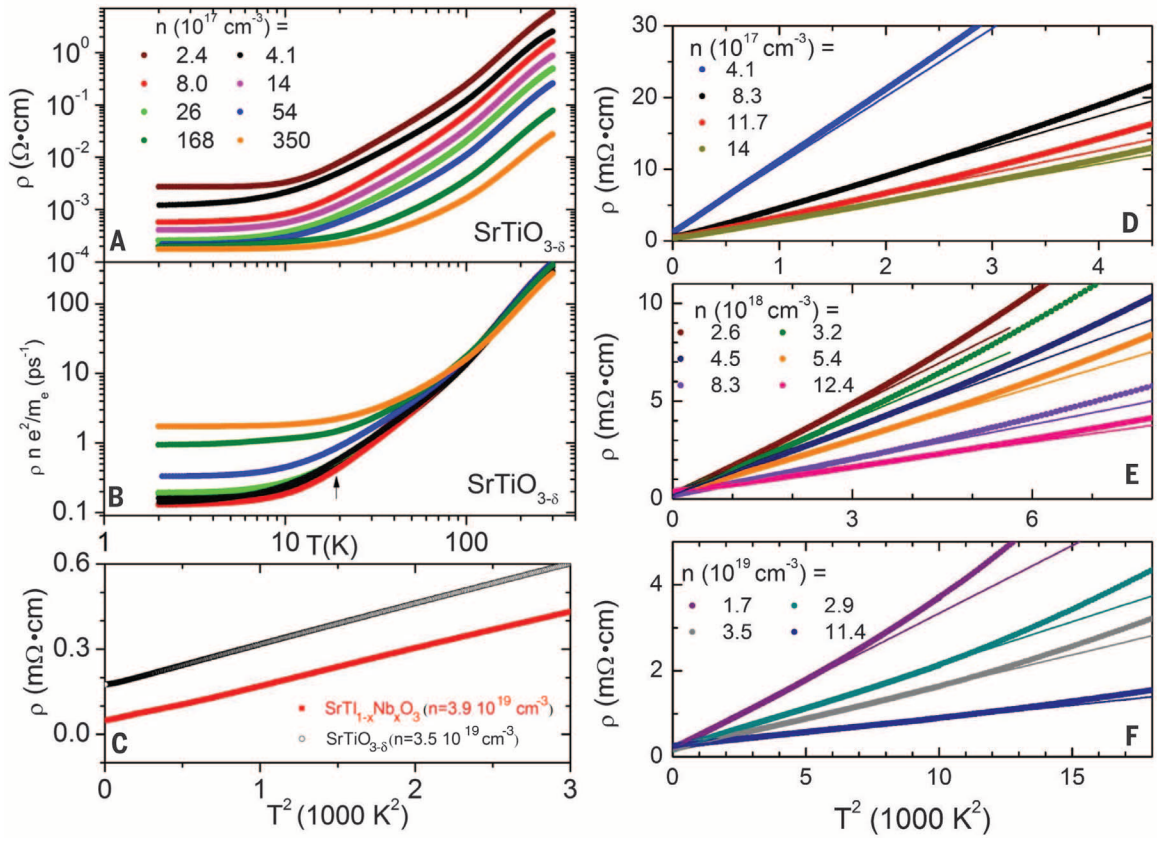

Fig. 1. Doping and temperature dependence of resistivity in n-doped $SrTiO_3$. (**A**) Evolution of resistivity in $SrTiO_{3-\delta}$ with doping across two orders of carrier density. (**B**) The product of resistivity and carrier density yields the scattering rate, which does not depend on carrier concentration above 100 K. (**C**) Resistivity plotted as a function of T^2 in oxygen-deficient and Nb-doped $SrTiO_3$ samples of comparable carrier concentration displays the same slope but different intercepts. (**D** to **F**) Resistivity versus T^2 in $SrTiO_{3-\delta}$ as the carrier density changes by two orders of magnitude. Straight solid lines represent the best fits to low-temperature data. As doping increases, the slope gradually decreases, and the upward deviation toward the phonon-dominated regime shifts to higher temperatures. Note the change in the vertical and horizontal scales with increasing carrier density.

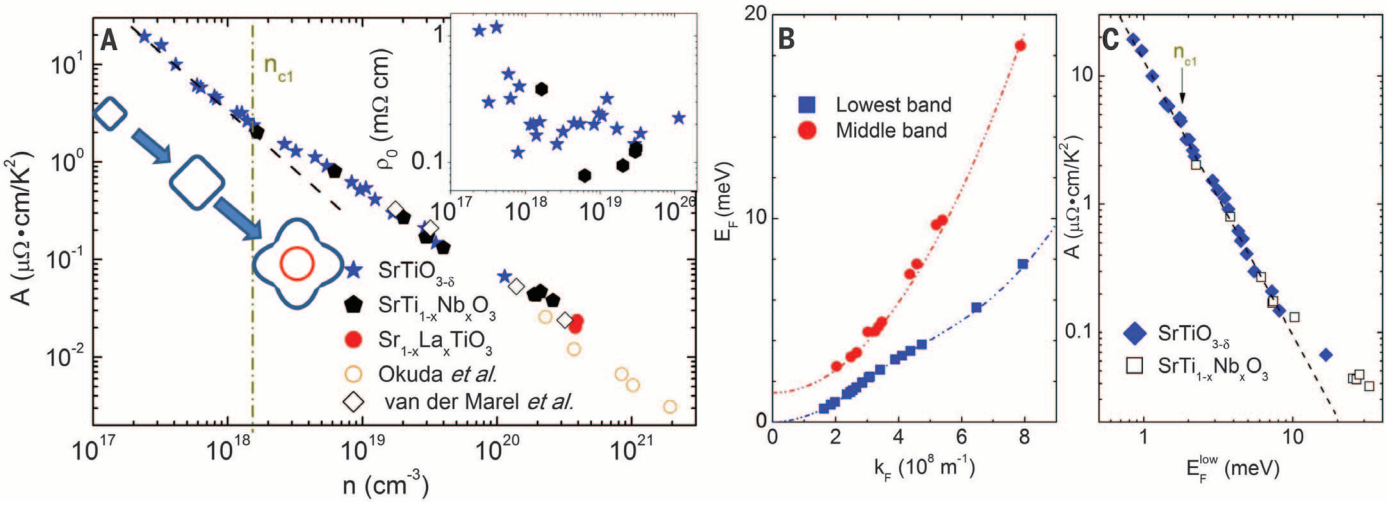

Fig. 2. Variation of *A* with carrier concentration and Fermi energy. (**A**) The prefactor *A* of T^2 resistivity as a function of carrier concentration on a log-log scale. The data represented by empty circles and diamonds are from (*12*) and (*13*), respectively. A dash-dot vertical line marks the first critical doping, above which a second band begins to be filled (*13*, *16*). The evolution of the Fermi surface with increasing concentration is also depicted here. Below n_{c1}, the Fermi surface is a simple squeezed ellipsoid, whereas above n_{c1} it has two concentric components with growing outer lobes. (Inset) Residual resistivity ρ_0 extracted from $\rho = \rho_0 + AT^2$ fits. (**B**) Dispersion of the two bands extracted from quantum-oscillation measurements (*16*). (**C**) Dependence of the prefactor *A* on the Fermi energy measured from the bottom of the lower band. Its dependence is close to E_F^{-2} across n_{c1}, with a deviation emerging at higher energies.

Here, $\hbar$ is Planck's constant h divided by 2π; e is the electron charge; and ℓ_{quad} is a material-dependent length scale, which can be set by the Fermi wavelength of electrons, the interatomic distance, or a combination of both. Mott argued that the average distance between two scattering events is proportional to the concentration and the collision cross section of electrons (σ_{cs}) (*7*). Therefore

$$A = \frac{\hbar}{e^2}\left(\frac{k_B}{E_F}\right)^2 k_F \sigma_{cs} \qquad (2)$$

Here, k_F is the Fermi wave vector, and σ_{cs} is set by the specific process governing the decay in charge current due to the presence of a lattice.

There are several types of theoretical proposals for generating T^2 resistivity from electron-electron scattering in the presence of a lattice. The first (*1*) invokes a multiband system with two different electron masses. Momentum transfer between these two distinct electron reservoirs sets the temperature dependence of resistivity, and the mass mismatch leads to a leak of momentum toward the lattice thermal bath. The second invokes Umklapp scattering and the fact that momentum conservation does not prohibit the transfer of a unit vector of the reciprocal lattice (*8*, *9*). In addition to these theories, Pal *et al.* have recently argued that Fermi liquids lacking Galilean invariance can display *T*-square resistivity, even in the absence of any Umklapp process (*10*), due to electron-impurity scattering. In addition to these semiclassic scenarios, quantum interference can also generate a resistivity proportional to $T^2 \ln T$ (*10*, *11*). The relevance of these ideas to the ubiquitous T^2 resistivity observed in a wide variety of Fermi liquids has not been settled experimentally.

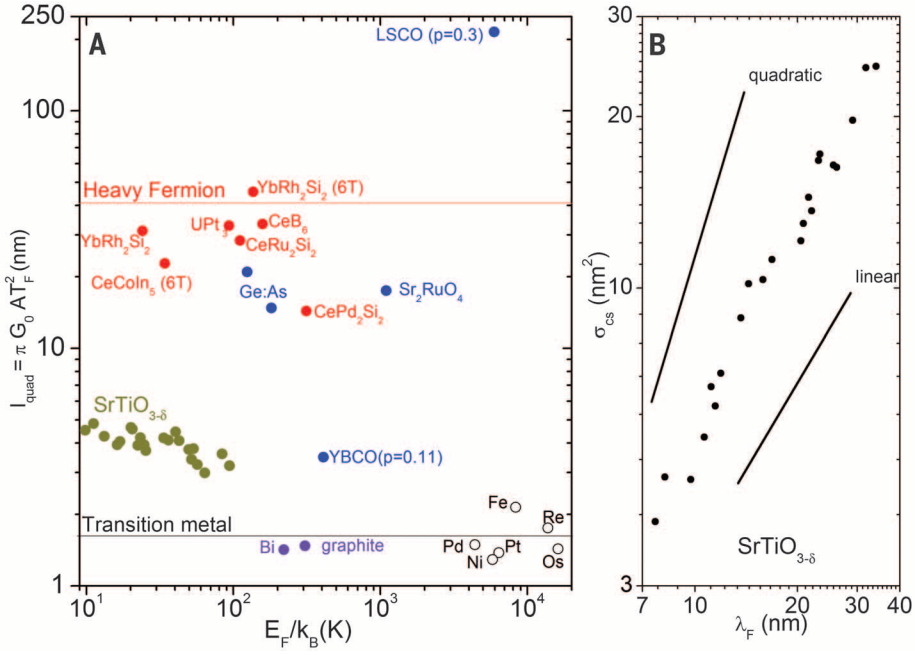

Fig. 3. Characteristic length scale of electron-electron scattering in $SrTiO_{3-\delta}$ compared with other Fermi liquids. (**A**) The length scale shown here is defined in Eq. 1 and extracted from *A* and T_F ($\ell_{quad} = \pi G_0 AT_F^2$, where $G_0 = 2e^2/h$) in $SrTiO_{3-\delta}$, as well as a number of other Fermi liquids (see tables S3 and S4 for details and references). The two horizontal solid lines correspond to the Kadowaki-Woods A/γ^2 ratio in heavy fermions (10 microhm·cm mol^2 K^2 J^{-2}; red) and transition metals (0.4 microhm·cm mol^2 K^2 J^{-2}; black) (*2*, *3*, *6*). LSCO, $La_{2-x}Sr_xCuO_4$; YBCO, $YBa_2Cu_3O_y$. (**B**) The extracted collision cross section of electrons (see Eq. 2) as a function of Fermi wavelength follows a dependence close to $\lambda_F^{1.2}$.

It has been known for two decades that n-doped $SrTiO_3$ with a carrier density exceeding 0.01 electrons per formula unit follows a T^2 resistivity (*12*). This T^2 resistivity provided input for the analysis of the Kadowaki-Woods ratio in low-density Fermi liquids (*5*) and the Landau quasiparticles of the polaron Fermi liquid (*13*). More recently, it has been reported that because of its exceptionally long Bohr radius, $SrTiO_3$ keeps a robust metallic resistivity down to very low doping levels (*14*). Moreover, both oxygen-deficient (*15*, *16*) and La-doped $SrTiO_3$ (*17*) host a well-defined

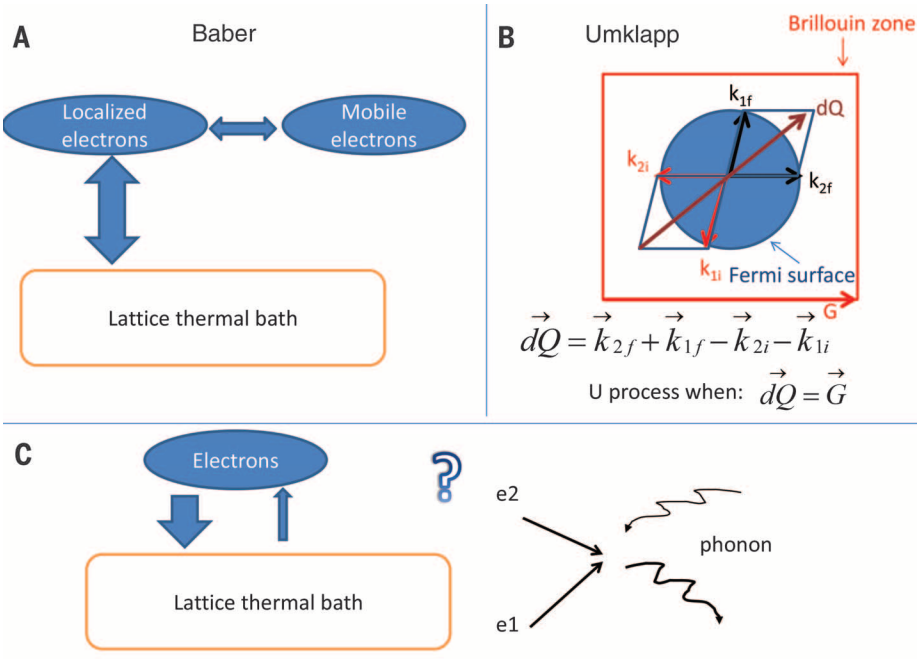

Fig. 4. Theoretical models for T^2 resistivity. (**A**) The original mechanism (*1*) requires two distinct reservoirs of electrons with different strengths of coupling to the lattice. (**B**) Umklapp scattering in which the momentum balance between incoming and outgoing electrons differs by a unit vector (k_{1i}, k_{2i}) of the reciprocal lattice. Such events are possible only when the Fermi wave vector (k_{1f}, k_{2f}) is equal to or larger than one-fourth the width of the Brillouin zone. $\vec{\mathbf{G}}$, reciprocal lattice vector; $\vec{\mathbf{dQ}}$, wave-vector imbalance between initial and final states. (**C**) Neither of these scenarios can explain the persistence of T^2 resistivity in the case of dilute $SrTiO_{3-\delta}$, in which there is a single tiny Fermi surface at the center of the Brillouin zone. A scenario is required in which (at least some) scattering events between electrons are accompanied by an asymmetric exchange of momentum with the lattice.

Fermi surface down to carrier densities as low as 3×10^{17} cm^{-3} (which corresponds to 2×10^{-5} electrons per formula unit. Such a context provides an opportunity to test the relevance of different theoretical pictures for the origin of T^2 resistivity.

Here we present resistivity measurements showing that the T^2 resistivity persists when the carrier density becomes two orders of magnitude lower than previously reported values (*12*, *13*). The magnitude of A varies smoothly as a function of E_F and becomes comparable to what has been seen in a heavy-fermion metal. The most important finding is the persistence of T^2 behavior in the single-band regime, where there is only a single electron reservoir with a Fermi wave vector much too small for any Umklapp process. This severely restrains possible origins of the observed T^2 resistivity. The experimental determination of the collision cross section of electrons in a Fermi liquid with a simple and well-documented Fermi surface topology provides a quantitative challenge for theory. Comparing the data obtained on n-doped $SrTiO_3$ with other Fermi liquids, we argue that ℓ_{quad}, the characteristic length scale of electron-electron scattering in each Fermi liquid, is a source of information regarding the microscopic origin of momentum decay.

The evolution of resistivity as carrier density changes from between 10^{17} and 10^{20} cm^{-3} is presented in Fig. 1 [see (*18*) for details on all 35 samples studied]. In agreement with previous reports (*14*–*17*, *19*), $SrTiO_3$ in this doping range is found to be a dilute metal whose resistivity drops by several orders of magnitude as it is cooled from room temperature to liquid helium temperatures.

Above 100 K, the scattering rate extracted from resistivity and carrier concentration [$\tau^{-1} = \frac{\rho n e^2}{m_e}$ (n, carrier density; m_e, free electron mass) in Fig. 1B] does not vary with doping and roughly follows a T^3 dependence (we are neglecting the mass renormalization, which would lead to a correction between 1.8 and 5 in this doping window). Below 100 K, inelastic resistivity evolves with carrier concentration. Both electron-phonon and electron-electron scattering mechanisms can depend on the size of the Fermi surface. In the case of acoustic phonons, as documented in graphene (*20*), the Bloch-Grüneisen temperature ($\Theta_{BG} = \frac{2\hbar v_s k_F}{k_B}$, where v_s is the sound velocity) separates two regimes. In a degenerate three-dimensional Fermi liquid, the inelastic resistivity caused by phonon scattering is expected to follow T^5 below Θ_{BG} and become T-linear above Θ_{BG}. In our case, Θ_{BG} and the Fermi degeneracy temperature are of the same order of magnitude. Therefore, at high temperatures, electrons scattered by phonons are obeying Boltzmann statistics. Here we focus on the T^2 inelastic resistivity emerging at low temperatures, which has been attributed to the scattering of electrons off of each other (*5*, *12*, *13*).

As seen in Fig. 1, D to F, the slope of the ρ-versus-T^2 plots for $SrTiO_{3-\delta}$ (δ quantifies the departure from stoichiometry due to the introduction of oxygen vacancies) smoothly decreases with increasing carrier concentration. In all cases, there is a deviation upward from the T^2 behavior toward a regime with a higher exponent. This is in contrast to the case of Fermi liquids with strong correlation, in which quasi-particles are destroyed by warming well below the degeneracy temperature. In $SrTiO_3$, the temperature at which the deviation occurs increases with doping. We found similar behavior in Nb-doped and La-doped $SrTiO_3$ (*18*). Fig. 2A shows the magnitude of A as a function of carrier concentration. Our data are compatible with those previously reported for higher carrier concentrations (*12*, *13*). Thus, decreasing carrier concentration is concomitant with a monotonous and uninterrupted increase in the magnitude of A across several orders of magnitude, as expected from Eq. 1. The residual resistivity ρ_0 (inset) varies much less with carrier concentration. Figure 1C shows that the magnitude of A is quasi-identical in two samples with identical carrier densities but different residual resistivities. Therefore, the magnitude of A is set by n and not by ρ_0.

In a Fermi liquid, the Fermi energy is reduced when the Fermi surface shrinks or when the effective mass is enhanced. In both cases, the magnitude of A is expected to increase, according to Eq. 1. Mass enhancement is the origin of the large A in heavy-fermion metals. Our results show that a large A can also be achieved by reducing the sheer size of the Fermi surface. In the extreme dilute limit, A becomes an order of magnitude larger than what is found in heavy-fermion UPt_3 (*21*).

Figure 2A reveals a hump in $A(n)$ near $n = 1.2 \times 10^{18}$ cm^{-3}. According to an extensive study of quantum oscillations (*16*), at this carrier density (dubbed n_{c1}), a second band begins to be filled and the cyclotron mass of the lowest band suddenly enhances. Figure 2B shows the energy dispersion in the two bands constructed from the frequency and effective mass obtained by quantum oscillations (*18*). The deviation from parabolicity in the lowest band occurs at $k = 0.4$ nm^{-1}, close to the expectations from the theoretical band structure, according to which anticrossing between bands generates a downward deviation of the lowest band near this wave vector (*13*).

The dispersion map of Fig. 2B allows us to determine the Fermi energy of each sample from its carrier density, leading to Fig. 2C, which shows A as a function of the Fermi energy of the lowest band with no visible anomaly near n_{c1}. The dependence remains close to E_F^{-2} over a wide range. This is a strong indication that the n_{c1} anomaly seen in Fig. 1A is almost entirely caused by deviation from parabolic dispersion in the lowest band, which hosts most of carriers.

As seen in fig. S1 (*18*), one can clearly detect a correlation between large A and small E_F across different materials by comparing the variation of A with Fermi energy in $SrTiO_{3-\delta}$ and in other Fermi liquids. The inclusion of dilute Fermi liquids in which the electronic specific heat is set by

the ratio of carrier density to Fermi energy is an extension of the Kadowaki-Woods approach.

Using Eq. 1, one can extract ℓ_{quad}, the characteristic length scale associated with electron-electron scattering in $SrTiO_{3-\delta}$. The extracted length (Fig. 3A) shows only a very slight decrease with doping and is not proportional to the Fermi wavelength (λ_F). A proportional relation between ℓ_{quad} and λ_F would have led to a $n^{-5/3}$ dependence of A in conformity with the simplest available treatments of electron-electron scattering (*22*, *23*).

Figure 3A compares the magnitude of ℓ_{quad} in $SrTiO_{3-\delta}$ with that of other Fermi liquids (see tables S3 and S4 for details). In a multicomponent Fermi surface, a complication arises because there is a multiplicity of Fermi energies. When the Fermi surface occupies a large fraction of the Brillouin zone, one can assume that there is roughly one electron per formula unit, and it is possible to extract the Fermi energy from γ. Thus, one can estimate the order of magnitude of ℓ_{quad} in dense heavy-fermion and transition metals. In Fig. 3A, these metal types lie close to the horizontal lines that represent the Kadowaki-Woods ratios in the two families (*2*–*6*). Figure 3A also includes data for the Fermi-liquid unconventional superconductor Sr_2RuO_4 (*24*), the heavily doped nonsuperconducting compound $La_{2-x}Sr_xCuO_4$ (*25*), and the $YBa_2Cu_3O_y$ cuprate at a doping level of $p = 0.11$ [in which resistivity is T^2 (*26*, *27*) and the Fermi energy of the small pocket seen by quantum oscillation has been quantified (*28*)]. We have also included reported data on bismuth (*29*), graphite (*30*), and arsenic-doped germanium (*31*). Figure 3A shows that ℓ_{quad} lies mostly between 1 and 40 nm. Its magnitude can be linked to the microscopic details of momentum decay by scattering in each system.

Using Eq. 2, we have also extracted the collision cross section of electrons in $SrTiO_{3-\delta}$ from the magnitude of A and the measured radius of the Fermi surface. Figure 3B shows variation of the collision cross section as a function of their Fermi wavelength. If the electrons were classical objects bouncing off of each other, σ_{cs} would have been $2\pi\lambda_F^2$. Our data are inconsistent with that classical picture; Fig. 3B shows that σ_{cs} is much smaller than $2\pi\lambda_F^2$ and does not follow λ_F^2. Hence, the theoretical challenge of providing a quantitative explanation for this observation remains.

The mechanism by which electron-electron scattering in Fermi liquids causes T^2 resistivity is not well understood. Previously, T^2 resistivity in Fermi liquids was observed in systems with a large single-component Fermi surface (such as $La_{1.7}Sr_{0.3}CuO_4$) or those with small multicomponent surfaces (such as bismuth or graphite). In each case, one of the scenarios shown in Fig. 4 could be ruled out, but one could still invoke either the multiplicity of reservoirs or the relevance of Umklapp processes. However, in the case of extremely dilute $SrTiO_{3-\delta}$, no room is left for either of the two. An Umklapp event cannot occur unless the largest available Fermi wave vector is one-fourth the size of the smallest vector of the reciprocal lattice, G. By a rough estimation, this corresponds to a carrier density of 2×10^{20} cm^{-3}, and Umklapp scattering may cause the hump in the energy dependence of $A(E_F)$ near 10 meV (see Fig. 2C), which corresponds to this carrier concentration. However, we find that A is still growing when k_F becomes 30 times smaller than G.

In the specific case of doped $SrTiO_3$, an explanation of the T^2 resistivity may invoke the polaronic nature of the quasi-particles (*13*) or the distorted structure of the Fermi surface (*17*). Beyond this particular case, our results highlight the absence of a microscopic theory for momentum decay through electron-electron scattering in different Fermi liquids. The magnitude of ℓ_{quad} can be experimentally quantified in each Fermi liquid. A potentially important role of phonon-assisted (*32*) electron-electron scattering should be reconsidered.

REFERENCES AND NOTES

1. W. G. Baber, *Proc. R. Soc. London Ser. A* **158**, 383–396 (1937).
2. M. J. Rice, *Phys. Rev. Lett.* **20**, 1439–1441 (1968).
3. K. Kadowaki, S. B. Woods, *Solid State Commun.* **58**, 507–509 (1986).
4. K. Miyake, T. Matsuura, C. M. Varma, *Solid State Commun.* **71**, 1149–1153 (1989).
5. N. E. Hussey, *J. Phys. Soc. Jpn.* **74**, 1107–1110 (2005).
6. A. C. Jacko, J. O. Fjaerestad, B. J. Powell, *Nat. Phys.* **5**, 422–425 (2009).
7. N. F. Mott, in *Metal-Insulator Transitions* (Taylor and Francis, London, ed. 2, 1990), pp. 72–73.
8. K. Yamada, K. Yosida, *Prog. Theor. Phys.* **76**, 621–638 (1986).
9. H. Maebashi, H. Fukuyama, *J. Phys. Soc. Jpn.* **67**, 242–251 (1998).
10. H. K. Pal, V. I. Yudson, D. L. Maslov, *Lith. J. Phys.* **52**, 142–164 (2012).
11. I. Paul, *Phys. Rev. B* **77**, 224418 (2008).
12. T. Okuda, K. Nakanishi, S. Miyasaka, T. Tokura, *Phys. Rev. B* **63**, 113104 (2001).
13. D. van der Marel, J. L. M. van Mechelen, I. I. Mazin, *Phys. Rev. B* **84**, 205111 (2011).
14. A. Spinelli, M. A. Torija, C. Liu, C. Jan, C. Leighton, *Phys. Rev. B* **81**, 155110 (2010).
15. X. Lin, Z. Zhu, B. Fauqué, K. Behnia, *Phys. Rev. X* **3**, 021002 (2013).
16. X. Lin *et al.*, *Phys. Rev. Lett.* **112**, 207002 (2014).
17. S. J. Allen *et al.*, *Phys. Rev. B* **88**, 045114 (2013).
18. See supplementary materials on *Science* Online.
19. A. Verma, A. P. Kajdos, T. A. Cain, S. Stemmer, D. Jena, *Phys. Rev. Lett.* **112**, 216601 (2014).
20. D. K. Efetov, P. Kim, *Phys. Rev. Lett.* **105**, 256805 (2010).
21. R. Joynt, L. Taillefer, *Rev. Mod. Phys.* **74**, 235–294 (2002).
22. W. E. Lawrence, J. W. Wilkins, *Phys. Rev. B* **7**, 2317–2332 (1973).
23. A. H. Thompson, *Phys. Rev. Lett.* **35**, 1786–1789 (1975).
24. A. P. Mackenzie, Y. Maeno, *Rev. Mod. Phys.* **75**, 657–712 (2003).
25. S. Nakamae *et al.*, *Phys. Rev. B* **68**, 100502(R) (2003).
26. D. LeBoeuf *et al.*, *Phys. Rev. B* **83**, 054506 (2011).
27. N. Barišić *et al.*, *Proc. Natl. Acad. Sci. U.S.A.* **110**, 12235–12240 (2013).
28. J. Chang *et al.*, *Phys. Rev. Lett.* **104**, 057005 (2010).
29. R. Hartman, *Phys. Rev.* **181**, 1070–1086 (1969).
30. D. T. Morelli, C. Uher, *Phys. Rev. B* **30**, 1080(R) (1984).
31. M. J. Katz, S. H. Koenig, A. A. Lopez, *Phys. Rev. Lett.* **15**, 828–830 (1965).
32. A. H. MacDonald, *Phys. Rev. Lett.* **44**, 489–493 (1980).

ACKNOWLEDGMENTS

We thank H. Maebashi, D. Maslov, and K. Miyake for stimulating discussions. This work was supported by Agence Nationale de Recherche through the SUPERFIELD and QUANTUM LIMIT projects and by a grant from the Ile de France region.

SUPPLEMENTARY MATERIALS

www.sciencemag.org/content/349/6251/945/suppl/DC1
Materials and Methods
Supplementary Text
Figs. S1 and S2
Tables S1 to S4
References (*33*–*60*)

6 February 2015; accepted 29 July 2015
10.1126/science.aaa8655

TOPOLOGICAL MATTER

Observation of chiral currents at the magnetic domain boundary of a topological insulator

Y. H. Wang,[1,2]* J. R. Kirtley,[1] F. Katmis,[3,4] P. Jarillo-Herrero,[4] J. S. Moodera,[3,4] K. A. Moler[1,2]*

A magnetic domain boundary on the surface of a three-dimensional topological insulator is predicted to host a chiral edge state, but direct demonstration is challenging. We used a scanning superconducting quantum interference device to show that current in a magnetized topological insulator heterostructure (EuS/Bi_2Se_3) flows at the edge when the Fermi level is gate-tuned to the surface band gap. We further induced micrometer-scale magnetic structures on the heterostructure and detected a chiral edge current at the magnetic domain boundary. The chirality of the current was determined by magnetization of the surrounding domain, and its magnitude by the local chemical potential rather than the applied current. Such magnetic structures provide a platform for detecting topological magnetoelectric effects and may enable progress in quantum information processing and spintronics.

The metallic surface of a three-dimensional topological insulator (3D-TI) is protected by time-reversal symmetry (TRS). Breaking TRS opens a band gap on the surface Dirac cone and transforms it into a Chern insulator (*1*–*4*). TRS-broken surface states are predicted to exhibit topological magneto-electric effects (*1*) and, when coupled with a superconductor, Majorana fermions (*5*–*7*). Just as the surface Dirac cone is a signature of the nontrivial

Science

Scalable T^2 resistivity in a small single-component Fermi surface

Xiao Lin, Benoît Fauqué and Kamran Behnia

Science **349** (6251), 945-948.
DOI: 10.1126/science.aaa8655

Trying to break a stubborn law

The electrical resistivity of most metals at low temperatures has a characteristic quadratic dependence on temperature. This law is typically ascribed to the scattering of electrons off each other in the presence of a crystal lattice. By measuring the resistivity of $SrTiO_3$ with varying dopant concentrations, Lin *et al.* test the applicability of the law for metals with low carrier densities. The law persists down to the lowest carrier concentrations, into the regime where the conditions for this behavior were previously thought to break down.

Science, this issue p. 945